Atmos. Chem. Phys. Discuss., 5, 10685–10721, 2005
www.atmos-chem-phys.org/acpd/5/10685/
SRef-ID: 1680-7375/acpd/2005-5-10685
European Geosciences Union

Atmospheric Chemistry and Physics Discussions

Spectroscopic evidence for β-NAT, STS, and ice in MIPAS infrared limb emission measurements of polar stratospheric clouds

M. Höpfner[1], B. P. Luo[2], P. Massoli[3], F. Cairo[3], R. Spang[4], M. Snels[3], G. Di Donfrancesco[5], G. Stiller[1], T. von Clarmann[1], H. Fischer[1], and U. Biermann[6,*]

[1]Forschungszentrum Karlsruhe, Institut für Meteorologie und Klimaforschung, Karlsruhe, Germany
[2]Institut für Atmosphäre und Klima, ETH-Hönggerberg, Zürich, Switzerland
[3]Consiglio Nazionale delle Ricerche, Istituto di Scienze dell'Atmosfera e del Clima, Rome, Italy
[4]Forschungszentrum Jülich, Institut für Chemie und Dynamik der Geosphäre, Jülich, Germany
[5]Ente per le Nuove tecnologie, l'Energie e l'Ambiente, Rome, Italy
[6]Max-Planck-Institut für Chemie, Abteilung Atmosphärenchemie, Mainz, Germany
[*]now at: Referat für Umwelt- und Energiepolitik des SPD-Parteivorstandes, Berlin, Germany

Received: 19 July 2005 – Accepted: 8 September 2005 – Published: 26 October 2005

Correspondence to: M. Höpfner (michael.hoepfner@imk.fzk.de)

Abstract

We have analyzed mid-infrared limb-emission measurements of polar stratospheric clouds (PSCs) by the Michelson Interferometer for Passive Atmospheric Sounding (MIPAS) during the Antarctic winter 2003 with respect to PSC composition. Coincident lidar observations from McMurdo were used for comparison with PSC types 1a, 1b and 2. By application of new refractive index data we could prove that a spectral signature at 820 cm^{-1} as observed by MIPAS near to the observation of a type 1a PSC is due to a composition of β-NAT. MIPAS infrared spectra collocated with Lidar observations of Type 1b and Type 2 PSCs could only be reproduced by assuming a composition of supercooled ternary $H_2SO_4/HNO_3/H_2O$ solution (STS) and of ice, respectively. Particle radius and number density profiles derived from MIPAS were generally consistent with the lidar observations. Only in the case of ice clouds, PSC volumes are underestimated due to large cloud optical thickness in the limb-direction. A comparison of MIPAS cloud composition and lidar PSC-type determination based on all available MIPAS-lidar coincident measurements revealed good agreement between PSC-types 1a, 1b and 2, and NAT, STS and ice, respectively. We could not find any spectroscopic evidence for the presence of nitric acid dihydrate (NAD) from any MIPAS observation of PSCs over Antarctica in 2003.

1. Introduction

Polar stratospheric clouds (PSCs) play an important role in the process of polar ozone depletion (Solomon, 1999). Through heterogeneous reactions they catalyze the conversion of chlorine from reservoir gases like $ClONO_2$ and HCl into active species which destroy ozone under sunlit conditions. Further, sedimentation of HNO_3 containing PSC particles leads to denitrification of the lower stratosphere, preventing fast reformation of $ClONO_2$ from active chlorine.

A classification of PSCs into different types was first achieved by observations with

ACPD

5, 10685–10721, 2005

Lidar instruments (Poole and McCormick, 1988; Browell et al., 1990; Toon et al., 1990). Type 2 clouds are characterized by high backscatter and depolarization ratios which are explained by ice particles. Type 1a and 1b clouds backscatter less light than Type 2. While 1a PSCs return a depolarized signal with relatively low backscatter ratio, Type 1b shows low depolarization and higher backscatter ratio, indicating large crystalline and small liquid particles, respectively.

In-situ and remote sensing measurements of total reactive nitrogen or gaseous HNO_3 have demonstrated that PSCs contain nitrate (Fahey et al., 1989; Arnold et al., 1989). Laboratory measurements and model calculations have shown that Type 1b particles most likely consist of supercooled ternary solution droplets of $H_2SO_4/HNO_3/H_2O$ (STS) (Carslaw et al., 1994; Tabazadeh et al., 1994) while nitric acid trihydrate (NAT) and other metastable hydrates of HNO_3 like nitric acid dihydrate (NAD) are candidates for Type 1a PSCs (Hanson and Mauersberger, 1988; Worsnop et al., 1993).

There exist very few direct measurements of the composition of PSC particles. In situ PSC measurements using balloon-borne mass spectrometers in the Arctic are consistent with either STS (Schreiner et al., 1999) or NAT (Voigt et al., 2000). However, these data were acquired within mountain wave-induced PSCs, so the findings cannot necessarily be generalized to the synoptic-scale PSCs that exist over large areas of Antarctica which experience much slower local heating and cooling rates (Schreiner et al., 1999). Thus, the composition of Type 1a PSCs is still not clarified completely (Tolbert and Toon, 2001).

A global view of PSC distribution is provided by satellite-borne observations. The Stratospheric Aerosol Measurement (SAM) II instrument was the first to measure the development of PSCs over the Arctic and Antarctic (McCormick, 1981). In these measurements PSC Types 1a and 1b could not be distinguished since the extinction had been measured in only one band in the near infrared (IR) at around 1 μm. However, for subsequent solar occultation instruments like the Polar Ozone and Aerosol Measurements (POAM) and the Stratospheric Aerosol and Gas Experiment (SAGE),

ACPD
5, 10685–10721, 2005

methods have been developed to discriminate between Type 1 PSCs on basis of different spectral channels in the visible and the near IR (Strawa et al., 2002; Poole et al., 2003). These methods rely on the assumption that Type 1b PSC particles are generally smaller than those of Type 1a, which results in a different wavelength dependence of the extinction coefficients.

Complementary to these size distribution-based methods, spectroscopic measurements in the mid-IR allow a distinction of PSC types on basis of their chemical composition by specific vibrational bands. Based on comprehensive laboratory investigations on refractive index data for possible PSC compositions (Toon et al., 1994) and aircraft-borne solar absorption measurements over Antarctica, NAT was ruled out as the likely composition of the observed PSCs (Toon and Tolbert, 1995). On the other hand, space-borne mid-infrared limb-emission observations by the CRyogenic Infrared Spectrometers and Telescopes for the Atmosphere (CRISTA) over Antarctica showed a distinctive spectral signature at around 820 cm^{-1} which was attributed to NAT through the observed temperature dependence (Spang and Remedios, 2003). However, this strong band could not be reproduced subsequently by available laboratory spectroscopic data on NAT. Also Höpfner et al. (2002) have reported a specific feature at 820 cm^{-1} in mid-IR spectra measured by the balloon-borne version of the Michelson Interferometer for Passive Atmospheric Sounding (MIPAS-B) which is also present in observations by the space-borne MIPAS on Envisat (Höpfner et al., 2004). Finally, Spang et al. (2005) found in a first comparison reasonable agreement between PSC-Type differentiation in MIPAS observations based on the 820 cm^{-1} band and SAGE III PSC type assignment in the Arctic winter 2002/2003.

We have analyzed measurements of PSCs by MIPAS during the Antarctic stratospheric winter 2003 when an aerosol Lidar at McMurdo station also had acquired data. Selected MIPAS/Lidar coincidences in which the Lidar had identified PSCs of one given type over its entire altitude range have been chosen to identify the chemical composition of the collocated MIPAS observations spectroscopically by detailed radiative transfer calculations including new refractive index data for NAT. MIPAS-derived PSC-types

ACPD
5, 10685–10721, 2005

have been compared with Lidar measurements over the whole Antarctic winter. Finally, we show results of an attempt to detect also nitric acid dihydrate (NAD) in MIPAS measurements.

2. Instruments

2.1. MIPAS

MIPAS on Envisat (Fischer and Oelhaf, 1996; ESA, 2000) is a limb-sounding spectrometer which detects the radiation from trace gases and particles in the atmosphere between 685 and 2410 cm^{-1} with an unapodized spectral resolution of 0.025 cm^{-1} (20 cm maximum optical path difference of the interferometer). The field-of-view is 30 km in the horizontal and about 3 km in the vertical at the tangent points. One limb scan of the standard observation mode covers the altitude range of 6–68 km in 17 steps with tangent altitude distances of 3 km for the 13 lower tangent altitudes, followed by 47 km, 52 km, 60 km and 68 km. These measurements cover the whole latitude band from pole to pole with 14.3 orbits per day and about 73 limb scans along one orbit. Sensitivity on optically thin clouds due to the long limb-pathway in combination with independence from any external light source enables, even at polar night, continuous observations of PSCs with full coverage of the Arctic and Antarctic regions.

During the period from mid-May until mid-October 2003 MIPAS operated quasi-continuously, with the exception of the periods 19–20 May, 25 May–4 June and 5–7 September, where no data are available. MIPAS observed PSCs in the Antarctic stratosphere during all days from 21 May until 15 October. The analysis in this paper is based on MIPAS spectra versions 4.57 and 4.59.

2.2. Lidar

The Lidar measurements which we used for selection and comparison with MIPAS data were performed from McMurdo Station (Ross Island, 77.9° S/166.7° E). The Lidar,

ACPD
5, 10685–10721, 2005

which is in operation for PSC monitoring since 1993, is a Nd:YAG system running at a wavelength of 532 nm (Adriani et al., 1992, 2004) where backscatter and depolarization data are acquired.

During the PSC period 2003 the Lidar operated from 22 May until 29 September. Due to instrumental problems from 4–11 June no depolarization measurements were possible. First PSCs over McMurdo were detected by 2 June and last ones at 19 September.

3. Spectroscopic analysis of single MIPAS/Lidar coincidences

3.1. Refractive indices

For modeling of MIPAS mid-IR spectra of PSCs, refractive index data from laboratory investigations are needed. We give a short overview of available optical constants and describe a new set of refractive indices for NAT.

Koehler et al. (1992) distinguished between two phases of crystalline NAT: α-NAT forms at temperatures below 185 K and und transforms irreversibly into β-NAT above about 188 K. Out of the gas-phase, β-NAT even crystallizes above 183 K (Tisdale et al., 1999). Thus, while α-NAT is metastable, β-NAT is the stable phase of NAT. Toon et al. (1994) provided the first optical constants of NAT in the IR. These were obtained by measuring the transmission through thin films, which were condensed out of the gas-phase at temperatures of 181 K for α-NAT and 196 K for β-NAT. A second set of refractive indices for α-NAT was determined by Richwine et al. (1995) through measurement of the extinction of particles nucleated homogeneously out of the gas phase at 160 K.

Figure 1A shows the imaginary parts of the refractive indices for the α-NAT data sets. The largest differences in the Toon et al. (1994) data compared to Richwine et al. (1995) are (1) the stronger absorption of the ν_3-Bande of NO_3^- at 1390 cm^{-1}, (2) the missing ν_2-band of H_3O^+ at 1120 cm^{-1}, and (3) the much weaker ν_2-band of NO_3^- at 820 cm^{-1}. To investigate these differences, Tisdale et al. (1999) measured absorption spectra of α-NAT films formed at different temperatures. They showed that

ACPD
5, 10685–10721, 2005

the spectrum observed at 162 K fitted better to the Richwine et al. (1995) data while at 180 K the measurement was more consistent with Toon et al. (1994). Tisdale et al. (1999) discussed two possible explanations for this observation: (1) there could exist spectroscopically different forms of α-NAT dependent on the temperature, or (2) α-NAT could be birefringent. Tisdale et al. (1999) concluded that in case of (1), for interpretation of PSC observations the optical constants by Toon et al. (1994) would be more suitable since these were measured at realistic temperatures. In case (2) none of the two datasets would be appropriate and it would be extremely difficult to reproduce real PSC observations by simulations.

We assume, however, that it is more likely that in the stratosphere the metastable α-NAT is converted to β-NAT or that β-NAT is formed directly. Figure 1B shows to our knowledge the only published optical constants of β-NAT by Toon et al. (1994). We derived two further sets of refractive indices for β-NAT from the work of Biermann (1998) who determined absorption spectra in a low-temperature cell. For the first measurement (labeled β-NAT[mol] in Fig. 1B) NAT was crystallized out of a 1:3 stoichiometric solution of HNO_3:H_2O (53.8 wt% HNO_3). For the second data set (β-NAT[coa]) NAT has been co-condensed together with ice out of the gas phase below the ice frost-point. After warming up to temperatures above the frost-point but still below the NAT existence temperature, pure NAT was grown from the gas-phase. Apart from a few differences, both measurements were attributed to β-NAT (Biermann, 1998) due to the stretching mode of OH at 3375 cm^{-1}, the stretching mode of the H_3O^+ ion at 2750 cm^{-1}, the bending mode of H_3O^+ at 1850 cm^{-1}, and the asymmetric stretching mode of the NO_3^- ion at 1375 cm^{-1}. From the β-NAT transmission spectra we derived refractive indices as described by Biermann et al. (2000). However, since the thickness of the NAT-film is not well known, it has been determined by a fit to the β-NAT data of Toon et al. (1994). The resulting absolute uncertainty in film thickness and, thus, in the refractive index is estimated to ±30% (Biermann, 1998).

An important aspect regarding the present work is the large intensity of the ν_2-band of NO_3^- (Ritzhaupt and Devlin, 1991) at 820 cm^{-1} compared to the previously reported

ACPD
5, 10685–10721, 2005

optical constants by Toon et al. (1994). Figure 2 shows this wavenumber region in detail. For comparing the spectra of such a relatively narrow band the spectral resolution of the measurements must be taken into account. While Biermann (1998) obtained the data with a resolution of 1 cm^{-1}, Toon et al. (1994) measured with 8 cm^{-1}. Thus, we degraded the new β-NAT indices to be consistent with the coarser spectral resolution. As shown in Fig. 2 the shape of the bands becomes more similar. The maximum intensity of the absorption feature is reduced by 40%, which is, however, still about a factor of 1.7 stronger than the observations by Toon et al. (1994). The reason for this is unknown.

In Fig. 1C we present available refractive indices for NAD by Toon et al. (1994) and Niedziela et al. (1998). Tisdale et al. (1999) attributed the differences to the existence of various NAD crystal structures depending on the formation conditions.

Figure 1D shows that refractive indices for ice are well known and, thus, are reliable for use in radiative transfer modelling.

Refractive indices for STS can be calculated by application of a mixing rule to the binary solutions of H_2SO_4/H_2O and of HNO_3/H_2O (Biermann et al., 2000). For volcanically unperturbed stratospheric conditions as in the case of the MIPAS observations in 2003, mainly the refractive index of HNO_3/H_2O determines the optical constants of STS PSCs with volume densities $\geq 1\,\mu m^3 cm^{-3}$. As an example in Fig. 1E we show refractive indices for 45 wt% solutions of HNO_3/H_2O by Biermann et al. (2000) and by Norman et al. (1999), respectively. Wagner et al. (2003) attributed the differences in band intensity between 1000 and 1700 cm^{-1} to a simplified analysis of the thin film spectra in Biermann et al. (2000). To simulate STS PSCs within MIPAS spectra we calculated refractive indices using the mixing rule by combining different sets of binary optical constants: (1) those provided by Biermann et al. (2000), and (2) HNO_3/H_2O by (Norman et al., 1999) combined with H_2SO_4/H_2O by Niedziela et al. (1999).

ACPD
5, 10685–10721, 2005

3.2. Radiative transfer and retrieval model

To calculate the radiative transfer of mid-IR limb measurements of PSCs it is necessary to account for radiation from the earth surface and the troposphere which is scattered by the particles into the direction of the instrument (Höpfner et al., 2002). We use the Karlsruhe Optimized and Precise Radiative transfer Algorithm (KOPRA) for the simulation of MIPAS/Envisat measurements (Höpfner, 2004). This code, which includes single scattering for a curved atmosphere, has been validated by comparison with a multiple scattering model (Höpfner and Emde, 2004). There it has been shown that clouds with IR limb optical thickness of PSCs can be modelled by single scattering within an error of a few percent.

KOPRA is embedded in a retrieval environment which allows to derive directly microphysical properties of particles from radiance spectra (Höpfner et al., 2002). Particle sizes are described by altitude dependent lognormal distributions defined by number density ($N(h)$), median radius ($r_m(h)$) and geometric standard deviation $\sigma(h)$:

$$n(r, h) = \frac{N(h)}{rs(h)\sqrt{2\pi}} \exp\left[-\frac{\ln^2(r/r_m(h))}{2\sigma(h)^2}\right], \quad (1)$$

where r is the particle radius and h the altitude.

Atmospheric profiles of aerosol parameters or trace gases are represented by the vector of unknown parameters, $\boldsymbol{x}$, which is determined in a Newtonian iteration process to account for the nonlinearity of the atmospheric radiative transfer (Rodgers, 2000; von Clarmann et al., 2003):

$$\boldsymbol{x}_{i+1} = \boldsymbol{x}_i + (\mathbf{K}^T\mathbf{S}_y^{-1}\mathbf{K} + \mathbf{R})^{-1} \times (\mathbf{K}^T\mathbf{S}_y^{-1}(\boldsymbol{y}_{\text{meas}} - \boldsymbol{y}(\boldsymbol{x}_i)) - \mathbf{R}(\boldsymbol{x}_i - \boldsymbol{x}_a)). \quad (2)$$

$\boldsymbol{y}_{\text{meas}}$ is the vector of selected measured spectral radiances of all tangent altitudes under investigation, and $\mathbf{S}_y$ is the related noise covariance matrix. $\boldsymbol{y}(\boldsymbol{x}_i)$ contains the spectral radiances calculated by the radiative transfer model using the best guess atmospheric state parameters $\boldsymbol{x}_i$ of iteration number i. $\mathbf{K}$ is the Jacobian matrix, i.e. the

ACPD
5, 10685–10721, 2005

partial derivatives $\partial \boldsymbol{y}(\boldsymbol{x}_i)/\partial \boldsymbol{x}_i$. **R** is a regularization matrix and $\boldsymbol{x}_a$ the a-priori information.

3.3. Data analysis

To deal with rather pure PSC types for the spectroscopic analysis we selected three MIPAS/Lidar coincidences in which the Lidar identified PSCs of either Type 1a, Type 1b, or Type 2 over its entire altitude range (see Table 1). Lidar backscatter and depolarization ratios for these examples are shown in Fig. 3. The chemical composition of these PSCs then was spectroscopically analyzed using the collocated MIPAS observations.

Following the scheme in Höpfner et al. (2002) we first determined altitude profiles of particle number density ($N(h)$ in Eq. 1) by non-linear least squares fitting of the MIPAS limb radiances in spectral windows centered at around 830 cm^{-1}, 950 cm^{-1} and 1220 cm^{-1} where trace-gas interference is low. The retrieval was performed on a 1 km grid between 12 and 29 km altitude with a 1st order smoothing constraint in **R** (Steck, 2002), and an initial guess $\boldsymbol{x}_0$ and a-priori $\boldsymbol{x}_a$ equal zero. The regularization strength was chosen such that five degrees-of-freedom are achieved. This is equivalent to an altitude resolution of about 3.4 km in terms of the full width at half maximum of the related column of the averaging kernal matrix

$$\mathbf{A} = (\mathbf{K}^T \mathbf{S}_y^{-1} \mathbf{K} + \mathbf{R})^{-1} \mathbf{K}^T \mathbf{S}_y^{-1} \mathbf{K}. \quad (3)$$

In this way number density profiles were determined for various height-constant median radii ($r_m(h)$) between 0.2 and 9 μm and for all sets of refractive indices described in Sect. 3.1. For STS we determined the altitude dependent refractive indices by using the mixing rule of Biermann et al. (2000). STS particle composition was calculated from thermodynamic equilibrium (Carslaw et al., 1994) based on ECMWF temperature analysis, 4–10 ppbv HNO_3, 3–5 ppmv H_2O and 0.3 ppbv H_2SO_4. The resulting altitude profiles of PSC number density will be discussed and compared with the collocated Lidar observations in Sect. 3.4 below.

ACPD
5, 10685–10721, 2005

Subsequently we determined abundances of trace gases with major spectroscopic signatures in the used MIPAS channels (O_3, H_2O, N_2O, CH_4, HNO_3, CFC-11) within specific spectral windows. Using these trace gas profiles together with the number densities and mean radii for which the best fit between radiative transfer calculations and measurements was obtained, we performed broadband spectral calculations for each refractive index data set.

Figure 4 shows results of such a calculation in comparison with MIPAS for a coincident MIPAS/Lidar measurement where the Lidar observed a PSC of Type 1a. We also show a PSC-free spectrum taken just northwards (black dotted line in 5th row of Fig. 4) to demonstrate the effect of PSCs on the radiances and to indicate the spectral influence of trace gas contribution. A strong spectral signature is present in the MIPAS PSC spectrum at around 820 cm^{-1}, clearly distinguishable from any trace gas signature. This feature can be reproduced using both sets of refractive indices for β-NAT derived from Biermann (1998). From these, β-NAT[coa] resulted in the best fit using a median particle radius of 0.8 μm. β-NAT[mol], for which the best fit has been obtained with a particle radius of 1.5 μm, reproduces the 820 cm^{-1} feature and the wavenumber region above about 1300 cm^{-1} slightly worse. The sensitivity of the fit on particle size is demonstrated by also showing the calculated spectrum for 0.8 μm in Fig. 4 which strongly deviates from the measurement between 900 and 960 cm^{-1}.

Refractive indices of α-NAT by Richwine et al. (1995) and β-NAT by Toon et al. (1994) provide a signature at around 820 cm^{-1}, but of much weaker intensity. Spectroscopic data of NAD, STS, and ice show no evidence of the observed spectral band. This agrees with simulations in the shorter wavelength channel B of MIPAS (see right part of Fig. 4). Here the calculations with all sets of refractive indices for β-NAT agree best with the measurements. Due to the much stronger ν_3-band of NO_3^- at around 1400 cm^{-1}, α-NAT calculations do not match the observed spectra there.

Analysis of MIPAS spectra for coincident data where the Lidar observed PSCs of Type 1b and 2 are shown in Figs. 5 and 6, respectively. In both cases the MIPAS measurements do not show a bandlike structure at 820 cm^{-1}.

ACPD
5, 10685–10721, 2005

For Type 1b (Fig. 5) best fits over the whole spectral range were obtained with refractive indices of STS. Both sets of refractive indices by Biermann et al. (2000) and Norman et al. (1999)/Niedziela et al. (1999) fit the observations. Thus, it cannot be decided which data set is superior.

In case of the Lidar Type 2 observation, the assumption of ice reproduces the MIPAS spectra best (Fig. 6).

3.4. Discussion of retrieved PSC altitude profiles

Figure 7 shows MIPAS retrievals of PSC number density profiles for those median radii and refractive indices for which best fits between measured and calculated spectra have been obtained. Volume densities are also shown, since, for small particles aerosol absorption is proportional to particles volume, while scattering can be neglected. Thus, N,r_m and σ are interdependent quantities. For particles larger than about 0.7 μm there is some independent information on radius (Höpfner, 2004), which is the reason that we obtain different spectral fit quality for variation of r_m. However, as has e.g. been shown by Echle et al. (1998), it is hardly possible to obtain independent information on the distribution width σ in addition to N and r_m. Thus, for our analysis, we have set σ to a constant value of 1.35.

Volume density from the retrieval can be compared to the volume solid or liquid PSC phases can reach under thermodynamic equilibrium conditions (Hanson and Mauersberger, 1988; Carslaw et al., 1995). We calculated these profiles using high southern latitude mean profiles of water vapor and HNO_3 from MIPAS retrievals in May 2003, temperature from ECMWF and 0.3 ppbv H_2SO_4 (named "Equil. (I)" in Fig. 7). In the Type 1a case the NAT equilibrium volume is largely overestimated above about 16 km compared to the retrieval. The reason for this are too large assumed HNO_3 abundances at these altitudes in the equilibrium calculation. The measurement took place on 4 August when HNO_3 had been depleted due to sedimentation of PSC particles in the previous two months. Thus we have used the actual gas-phase HNO_3 profile determined from MIPAS to calculate the profile "Equil. (II)" in Fig. 7. The results fit much

ACPD
5, 10685–10721, 2005

better to the low values above about 19–20 km which means that PSC formation was strongly suppressed there. Below 15 km the retrieval shows larger volume densities than the calculations which might be due to increased values of HNO_3 as result of vertical redistribution from particle sedimentation. The actual HNO_3 profile of MIPAS cannot help here to improve the calculation because it gives only information about the gas-phase concentrations.

Calculated and retrieved volume densities fit reasonably well in case of the PSC Type 1b observation. There is some overestimation above about 19 km which might be caused by ECMWF temperatures which often are too low at these altitudes in this period as has been shown by comparison with radiosonde measurements (P. von der Gathen, pers. comm.).

Retrieved volume densities from the PSC Type 2 observations are much smaller than those obtained from equilibrium calculations. This is caused by ice PSCs becoming close to optically thick in mid-IR limb observations such that no information can be retrieved any more. However, from the broadband spectral comparison we have seen that for the tangent altitude at the cloud top there is some information. This will also be shown in the following comparison with the Lidar measurements.

To compare MIPAS PSC profiles with the collocated Lidar measurements we determined the aerosol backscatter coefficients at the Lidar wavelength of 532 nm by Mie calculations using lognormal size distributions with $N(h)$, r_m and σ from MIPAS. Available refractive indices for PSCs show some variation, especially for NAT and STS. In case of NAT Middlebrook et al. (1994) measured values of 1.51 for α-NAT and a lower limit of 1.46 for β-NAT at 632 nm in the laboratory. These are consistent with the range of 1.46–1.54 at 532 nm Deshler et al. (2000) derived from balloon-borne observations of a depolarizing PSC-layer. However, recently Scarchilli et al. (2005) state refractive indices for NAT of 1.37–1.45. For STS Deshler et al. (2000) calculated values in the range 1.43–1.49 at 532 nm which is, on average, slightly higher than values expected from theory (1.43) for this observation (Luo et al., 1996). Even higher values for STS have been reported by Larsen et al. (2000): 1.5 at 940 nm, and by Scarchilli et al.

ACPD
5, 10685–10721, 2005

(2005): 1.51–1.55 at 532 nm. Refractive indices for ice are more consistent: e.g. 1.30 (Middlebrook et al., 1994) or 1.31–1.33 (Scarchilli et al., 2005). To cover this variability, we used refractive indices of 1.37–1.54 for Type 1a, 1.43–1.55 for Type 1b and 1.30–1.33 for Type 2 for the calculations in Fig. 8.

In case of the MIPAS-Lidar Type 1a match, backscatter coefficient profiles have been calculated for the MIPAS result of $N(h)$ with r_m=0.8 μm which was the best result of radius for the Biermann (1998) [coa] data and r_m=1.5 μm, the result for the Biermann (1998) [mol] dataset (see Fig. 4). Using the smaller radius the calculated backscatter coefficients exceeded the lidar data by about a factor of 5, while for r_m=1.5 μm there is good agreement between lidar and MIPAS (Fig. 8, left panel). This might be an indication that the Biermann (1998) [mol] refractive index dataset is more appropriate for quantitative analysis of MIPAS Type 1a observations.

As mentioned above, there is no independent information on the particle sizes in MIPAS observations of small particles. Therefore, in case of Type 1b PSCs r_m=0.1, 0.2 or even 0.5 μm lead to fits between calculated and measured spectra of comparable quality. The middle panel in Fig. 8 shows that the lidar data can best be reproduced with r_m=0.1 μm. However, also r_m=0.2 μm leads to similar results if the smaller refractive indices from literature (1.43) of STS at 532 nm are used.

For the example of a Type 2 PSC we already stated that volume density is strongly underestimated due to cloud opacity in limb-direction. This is also the case when comparing the aerosol backscatter coefficients in Fig. 8, right panel. In the center of the cloud, backscatter coefficients calculated from MIPAS are much lower than lidar. However, at cloud top, above about 21 km altitude, calculated and measured coefficients agree quite well. This strengthens the argument that the observations contain information there. Thus, it is possible to distinguish spectroscopically the PSC composition as shown in Fig. 6 for a tangent altitude of 23.4 km.

4. Comparison of PSC types between all MIPAS/Lidar collocations

We now compare PSC Types observed by MIPAS and McMurdo lidar during the Antarctic winter period 2003. In order to differentiate the PSC composition directly from MIPAS spectra in a time-efficient way, i.e. such that no explicit forward-model runs are necessary, we have applied the method Spang and Remedios (2003) used to analyze PSC observations by CRISTA. This color-ratio method discriminates measurements with the spectral band signature of NAT at 820 cm^{-1} by plotting the ratio of the radiances at around 820 cm^{-1} and 792 cm^{-1} versus the cloud index CI, i.e. the ratio of radiances at 792 cm^{-1} and 832 cm^{-1}.

Figure 9 shows a color-ratio plot generated by radiative transfer calculations. We have used PSC number densities for a variety of temperature profiles covering the range of variability in the Antarctic stratosphere, derived via equilibrium calculations and for different supersaturations and different median particle radii. Region R1 contains only points from spectra calculated for β-NAT (red symbols). PSCs with a median particle radii of up to 2 μm fall into R1. For larger particles, the 820 cm^{-1} signature flattens and, thus, it cannot be separated from STS or ice any more. Region R3, i.e. points with values of CI<1.3 lying below the NAT-separation curve contain nearly exclusively ice PSCs. In R4 PSCs of STS, ice and large (>3 μm radius) NAT particles appear. Finally in R2 (CI>1.7) there are mainly STS and large NAT, but only few ice cases. Thus, the presence of NAT (R1) and ice (R3) can definitively be deduced from such a plot, whereas it is most difficult to distinguish STS, large NAT and ice in R4.

The detection limit for PSCs from MIPAS has been set to CI=4.5 which is in accordance with the value Spang and Remedios (2003) have used, i.e. for CI <4.5 a PSC is detected in the measurement. Our simulations show that this value is equivalent with a detection limit of PSCs with volume densities of 0.2–0.4 $\mu m^3 cm^{-3}$. This means that nearly no PSCs with volume densities less than 0.2 $\mu m^3 cm^{-3}$ are seen while for values larger than 0.4 $\mu m^3 cm^{-3}$ all PSCs are detected.

For the comparison we have selected MIPAS limb-scans closer than Δt=8 h and

ACPD
5, 10685–10721, 2005

Δd=800 km to the lidar measurements. This frequently results in multiple MIPAS matches per lidar observation. We have ordered these matches for increasing values of Δtot [km]=Δd [km]+100 km/h×Δt [h]. Figure 10 shows the comparison between the PSC-type altitude profiles from lidar and MIPAS from mid-June until mid-September 2003. For MIPAS the results of the collocated limb-scans with smallest (MIPAS 1) and second smallest (MIPAS 2) Δtot are given. Lidar PSC types have been derived by visual inspection of all backscatter and depolarization profiles and are identified by different colors. For MIPAS we have used the color ratio method and distinguished the different regions in Fig. 9 by different colors in Fig. 10.

The lidar sequence indicates that Type 1a PSCs were the most frequent type of clouds above McMurdo during the winter. Pure Type 1b clouds were only observed on 15 June (labeled A in Fig. 10). During few other days Type 1b signals were detected at distinct altitudes. Type 2 PSCs were present during three periods/days: 19–21 June (B), 15 July (D), and 12 August (H). These ice observations are well correlated with low temperatures over McMurdo (lower part of Fig. 10)

MIPAS-derived composition profiles match this general picture: mostly NAT was observed. On 15 June STS was seen, and ice was identified on all occasions when lidar detected Type 2 clouds. Regarding cloud top height, both instruments agree quite well until the second half of July. Afterwards lidar generally detected clouds higher up than MIPAS. This is due to the detection limit of MIPAS for clouds with low volume densities (see above). Such clouds which appear mainly in the second half of the winter can still be seen by lidar. In the following, exceptions are discussed where lidar-types do not match MIPAS-compositions.

On 23–24 June (C) lidar observed Type 1a PSCs over McMurdo during three measurements while MIPAS saw NAT only above 24 km. For the tangent altitudes below, there is indication for ice or STS and pure ice by MIPAS. Investigation of the related MIPAS spectra shows strong radiance signals typically for dense ice clouds. The surrounding MIPAS measurements on both days indicate, that McMurdo had been located close to a region of ice PSCs in the south. Also temperature over the station had still

ACPD
5, 10685–10721, 2005

been low. Thus, it is very probable that MIPAS measurements were influenced by ice PSCs during this period.

On 16–18 July (E), differences between lidar and MIPAS also appeared soon after a co-incident sighting of ice clouds (D). Thus, the situation was very similar to that on 23–24 June (C).

In one profile on 25–26 July (F) the "closest" selected limb-scan "MIPAS 1", being 1.5 h and 100 km off McMurdo, indicates STS above about 18 km while lidar detected STS only at the top of the profile. However, the related "MIPAS 2" measurement (Δt=0.1 h, Δd=600 km), shows NAT. Further, in the second profile of "MIPAS 2" ice was detected, indicating that McMurdo was again located in a transition zone, thus complicating comparison of PSC-types between lidar and MIPAS.

On 8 August (G), lidar observed a Type 1b PSC from about 12 to 17.5 km altitude with a Type 1a cloud on top. Interestingly here MIPAS also detected NAT above a layer which falls, due to its relatively large optical depth, into R4 in the radiance-ratio plot, and thus, could wrongly be taken for an ice PSC.

On 15–16 August (I) lidar detected Type 1a while we derived for "MIPAS 1" various compositions. Even signals as optically thick as ice were present. "MIPAS 2" is more in accordance with lidar. We propose that the reason for this were inhomogeneous nacreous clouds caused by mountain wave activity which were observed near McMurdo during these days.

Such nacreous clouds may also be the reason for the enhanced radiances in MIPAS data on 24 and 26 August. In this period (J), however, the clouds were near the MIPAS detection limit which presumably lead to problems in determination of PSC composition.

5. Search for NAD

Due to its lower energy barrier for nucleation compared to NAT, NAD has been proposed as a possible component of Type 1a PSCs (Worsnop et al., 1993; Tabazadeh

ACPD
5, 10685–10721, 2005

et al., 2001; Carslaw et al., 2002). We investigated whether there is spectroscopic evidence for NAD in MIPAS PSCs observations during the Antarctic winter of 2003.

Refractive indices (Fig. 1) and radiative transfer simulations for NAD (Fig. 4) show a prominent spectral signature at 810 cm^{-1} which is clearly distinguished from the NAT band at 820 cm^{-1}. We performed simulations of NAD spectra for various particle size distributions and plotted radiance ratios in the same manner as for the NAT detection (Fig. 11A). For these simulations the refractive indices of NAD by Niedziela et al. (1998) have been used because these were measured with a better spectral resolution (2 cm^{-1}) than the data by Toon et al. (1994) (8 cm^{-1}) and, thus, probably represent better the sharp spectral feature.

The calculations in Fig. 11A show that it should be possible to detect NAD in MIPAS spectra for particle distributions with median radii up to about 1 μm. For larger particles the prominent feature at 810 cm^{-1} disappears. Comparison with the same plot derived from measurements (Fig. 11B) reveals no indication of a strong band of NAD in any MIPAS PSC spectra we have investigated. Only 1.8% of all 7641 PSC observations lie slightly above the separation curve. We could not identify any specific NAD signature through visual inspection of individual spectra either. From this observation and the MIPAS PSC detection limit discussed above we conclude that no PSCs consisting of NAD particles with radii smaller than about 1 μm and volume densities larger than about 0.3 $\mu m^3/cm^{-3}$ were present in the observed airmasses in the Antarctic stratosphere during 2003.

6. Summary and conclusions

By detailed radiative transfer modeling we have demonstrated that a prominent spectral band at 820 cm^{-1} in MIPAS spectra of a PSC of Type 1a could best be modeled by the application of refractive index data of β-NAT derived from measurements by Biermann et al. (2000). Apart from this spectrally sharp feature, the β-NAT indices by Toon et al. (1994) also result in a good fit between measurement and simulation. It was not

ACPD
5, 10685–10721, 2005

possible to get any satisfactory fit with spectroscopic data of NAD, ice or STS.

However, we cannot definitively decide which of the new datasets for β-NAT is more appropriate for the simulation of NAT observations in the mid-IR. On the one hand, β-NAT[coa] results in the best fit to the measured spectrum and is more similar to previous optical constants of β-NAT (Toon et al., 1994). On the other hand, the two datasets lead to different results for particle size ([coa] 0.8 μm and [mol] 1.5 μm median radius). We have shown that aerosol backscatter coefficients at 532 nm calculated on basis of MIPAS results for r_m=1.5 μm agree better with collocated lidar observations. MIPAS spectra matching two lidar examples of Type 1b and Type 2 PSCs do not show the 820 cm^{-1}-band and could well be simulated with refractive indices of STS and ice, respectively.

By simulations on basis of the new refractive indices we have analysed a color-ratio method which had been derived empirically from CRISTA measurements to separate PSC types (Spang and Remedios, 2003). We have shown that NAT particles with radii smaller than about 3 μm and volume densities larger than about 0.3 $\mu m^3 cm^{-3}$ can be identified. Also dense ice clouds are easily distinguished while it is more difficult to differentiate between thinner ice clouds (e.g. not covering the entire field-of-view of MIPAS) and dense STS PSCs. The method has been applied to MIPAS measurements collocated with lidar PSC observations from McMurdo. In general we found good agreement between PSC type identification from lidar and the separation based on the MIPAS color ratio method. Differences are mainly attributed to temporal or spatial inhomogeneities of PSC-types and to the detection limit of MIPAS. Additionally, mixed-phase clouds pose potential problems to the detection scheme. We suppose that in general the type with the largest volume density over the field-of-view of MIPAS will be detected. A detailed analysis is envisaged in future.

The color ratio method has also been applied to search for the spectral signals of NAD in MIPAS observations. We found no definite evidence and conclude that very likely no NAD PSCs with median particle radii of less than 1 μm and volume densities larger than about 0.3 $\mu m^3/cm^{-3}$ existed over Antarctica 2003.

ACPD
5, 10685–10721, 2005

The present work is the basis for an analysis of the evolution of PSC-types during the onset of PSC activity in the Antarctic polar vortex in May and June 2003 which is reported in a companion paper (Höpfner et al., 2005).

Acknowledgements. Authors of this work were supported by the German HGF-Vernetzungsfonds ENVISAT (BMBF 01SF9953/8). MIPAS spectra were provided by the European Space Agency and meteorological data by ECMWF via NILU. Lidar measurements were supported by the Italian Programma Nazionale di Ricerche in Antartide. Gratitude is extended to the US National Science Foundation for making McMurdo Station available for the lidar measurements and for supplying winter-over science technical support. Related to this, we especially thank T. Deshler for his support.

References

Adriani, A., Deshler, T., Gobbi, G. P., Johnson, B. J., and Di Donfrancesco, G.: Polar stratospheric clouds over McMurdo, Antarctica, during the 1991 spring: Lidar and particle counter measurements, Geophys. Res. Lett., 19, 1755–1758, 1992. 10690

Adriani, A., Massoli, P., Di Donfrancesco, G., Cairo, F., Moriconi, M. L., and Snels, M.: Climatology of polar stratospheric clouds based on lidar observations from 1993 to 2001 over McMurdo Station, Antarctica, J. Geophys. Res., 109(D24), D24 211, doi:10.1029/2004JD004800, 2004. 10690

Arnold, F., Schlager, H., Hoffmann, J., Metzinger, P., and Spreng, S.: Evidence for stratospheric nitric acid condensation from balloon and rocket measurements in the Arctic, Nature, 342, 493–497, 1989. 10687

Biermann, U. M.: Gefrier- und FTIR-Experimente zur Nukleation und Lebensdauer stratosphärischer Wolken, Ph.D. thesis, Universität Bielefeld, cuvillier Verlag, ISBN 3-89712-212-X, 1998. 10691, 10692, 10695, 10698, 10712, 10717, 10719

Biermann, U. M., Luo, B. P., and Peter, T.: Absorption spectra and optical constants of binary and ternary solutions of H_2SO_4, HNO_3, and H_2O in the mid infrared at atmospheric temperatures, J. Phys. Chem. (A), 104, 783–793, 2000. 10691, 10692, 10694, 10696, 10702, 10717, 10719

Browell, E. V., Butler, C. F., Ismail, S., Robinette, P. A., Carter, A. F., Higdon, N. S., Toon,

O. B., Schoeberl, M. R., and Tuck, A. F.: Airborne lidar observations in the wintertime Arctic stratosphere: polar stratospheric clouds, Geophys. Res. Lett., 17, 385–388, 1990. 10687
Carslaw, K. S., Luo, B. P., Clegg, S. L., Peter, T., Primblecombe, P., and Crutzen, P. J.: Stratospheric aerosol growth and HNO_3 gas phase depletion from coupled HNO_3 and water uptake by liquid particles, Geophys. Res. Lett., 21, 2479–2482, 1994. 10687, 10694
Carslaw, K. S., Luo, B., and Peter, T.: An analytic expression for the composition of aqueous HNO_3–H_2SO_4 stratospheric aerosols including gas phase removal of HNO_3, Geophys. Res. Lett., 22, 1877–1880, 1995. 10696
Carslaw, K. S., Kettleborough, J. A., Northway, M. J., Davies, S., Gao, R., Fahey, D. W., Baumgardner, D. G., Chipperfield, M. P., and Kleinböhl, A.: A vortex-scale simulation of the growth and sedimentation of large nitric acid hydrate particles, J. Geophys. Res., 107(D20), SOL 43-1, 8300, doi:10.1029/2001JD000467, 2002. 10702
Deshler, T., Nardi, B., Adriani, A., Cairo, F., Hansen, G., Fierli, F., Hauchecorne, A., and Pulvirenti, L.: Determining the index of refraction of polar stratospheric clouds above Andoya (69° N) by combining size-resolved concentration and optical scattering measurements, J. Geophys. Res., 105, 3943–3954, 2000. 10697
Echle, G., von Clarmann, T., and Oelhaf, H.: Optical and microphysical parameters of the Mt. Pinatubo aerosol as determined from MIPAS–B mid–IR limb emission spectra, J. Geophys. Res., 103, 19 193–19 211, 1998. 10696
ESA: Envisat MIPAS: An instrument for atmospheric chemistry and climate research, Tech. Rep. SP-1229, European Space Agency, SA Publications Division, ESTEC, P. O. Box 299, 2200 AG Noordwijk, The Netherlands, 2000. 10689
Fahey, D. W., Murphy, D. M., Kelly, K. K., Ko, M. K. W., Proffitt, M. H., Eubank, C. S., Ferry, G. V., Loewenstein, M., and Chan, K. R.: Measurements of Nitric Oxide and Total Reactive Nitrogen in the Antarctic Stratosphere: Observations and Chemical Implications, J. Geophys. Res., 94, 16 665–16 681, 1989. 10687
Fischer, H. and Oelhaf, H.: Remote sensing of vertical profiles of atmospheric trace constituents with MIPAS limb-emission spectrometers, Appl. Opt., 35, 2787–2796, 1996. 10689
Hanson, D. and Mauersberger, K.: Laboratory studies of the nitric acid trihydrate: Implications for the south polar stratosphere, Geophys. Res. Lett., 15, 855–858, 1988. 10687, 10696
Höpfner, M.: Study on the impact of polar stratospheric clouds on high resolution mid–IR limb emission spectra, J. Quant. Spectrosc. Radiat. Transfer, 83, 93–107, 2004. 10693, 10696
Höpfner, M. and Emde, C.: Comparison of single and multiple scattering approaches for the

simulation of limb–emission observations in the mid–IR, J. Quant. Spectrosc. Radiat. Transfer, 91, 275–285, 2004. 10693

Höpfner, M., Oelhaf, H., Wetzel, G., Friedl-Vallon, F., Kleinert, A., Lengel, A., Maucher, G., Nordmeyer, H., Glatthor, N., Stiller, G. P., von Clarmann, T., Fischer, H., Kröger, C., and Deshler, T.: Evidence of scattering of tropospheric radiation by PSCs in mid–IR limb emission spectra: MIPAS–B observations and KOPRA simulations, Geophys. Res. Lett., 29(8), 119-1, 1278, doi:10.1029/2001GL014443, 2002. 10688, 10693, 10694

Höpfner, M., von Clarmann, T., Fischer, H., Glatthor, N., Grabowski, U., Kellmann, S., Kiefer, M., Linden, A., Tsidu, G. M., Milz, M., Steck, T., Stiller, G. P., and Wang, D.-Y.: Determination of PSC properties from MIPAS/ENVISAT limb emission measurements during the Antarctic winter 2003, in OZONE, Proceedings of the XX Quadrennial Ozone Symposium, edited by: Zerefos, C. S., International Ozone Commission, Athens, Greece, 974–975, 2004. 10688

Höpfner, M., Larsen, N., Spang, R., Luo, B. P., Ma, J., Svendsen, S. H., Eckermann, S. D., Knudsen, B., Massoli, P., Cairo, F., Stiller, G., v. Clarmann, T., and Fischer, H.: MIPAS detects Antarctic stratospheric belt of NAT PSCs caused by mountain waves, Atmos. Chem. Phys. Discuss., 2005, SRef-ID: 1680-7375/acpd/2005-5-10723. 10704

Koehler, B. G., Middlebrook, A. M., and Tolbert, M. A.: Characterization of model polar stratospheric cloud films using Fourier transform infrared spectroscopy and temperature programmed desorption, J. Geophys. Res., 97, 8065–8074, 1992. 10690

Larsen, N., Mikkelsen, I., Knudsen, B. M., Schreiner, J., Voigt, C., Mauersberger, K., Rosen, J. M., and Kjome, N. T.: Comparison of chemical and optical in situ measurements of polar stratospheric cloud particles, J. Geophys. Res., 105, 1491–1502, 2000. 10697

Luo, B., Krieger, U. K., and Peter, T.: Densities and refractive indices of $H_2SO_4/HNO_3/H_2O$ solutions to stratospheric temperatures, Geophys. Res. Lett., 23, 3707–3710, 1996. 10697

McCormick, M. P.: High-latitude stratospheric aerosol measured by the SAM II satellite system in 1978 and 1979, Science, 214, 328–331, 1981. 10687

Middlebrook, A. M., Berland, B. S., George, S. M., Tolbert, M. A., and Toon, O. B.: Real refractive indices of infrared-characterized nitric-acid/ice films: Implications for optical measurements of polar stratospheric clouds, J. Geophys. Res., 99, 25 655–25 666, 1994. 10697, 10698

Niedziela, R. F., Miller, R. E., and Worsnop, D. R.: Temperature- and frequency-dependent optical constants for nitric acid dihydrate from aerosol spectroscopy, J. Phys. Chem. (A),

102, 6477–6484, 1998. 10692, 10702, 10721
Niedziela, R. F., Norman, M. L., DeForest, C. L., Miller, R. E., and Worsnop, D. R.: A Temperature- and Composition-Dependent Study of H_2SO_4 Aerosol Optical Constants Using Fourier Transform and Tunable Diode Laser Infrared Spectroscopy, J. Phys. Chem. (A), 103, 8030–8040, 1999. 10692, 10696
Norman, M. L., Qian, J., Miller, R. E., and Worsnop, D.: Infrared complex refractive indices of supercooled liquid HNO_3/H_2O aerosols, J. Geophys. Res., 104, 30 571–30 584, 1999. 10692, 10696
Poole, L. R. and McCormick, M. P.: Airborne lidar observations of Arctic polar stratospheric clouds: Indications of two distinct growth stages, Geophys. Res. Lett., 15, 21–23, 1988. 10687
Poole, L. R., Trepte, C. R., Harvey, V. L., Toon, G. C., and VanValkenburg, R. L.: SAGE III observations of Arctic polar stratospheric clouds – December 2002, Geophys. Res. Lett., 30(23), A11, 2216, doi:10.1029/2003GL018496, 2003. 10688
Richwine, L. J., Clapp, M. L., Miller, R. E., and Worsnop, D. R.: Complex refractive indices in the infrared of nitric acid trihydrate aerosols, Geophys. Res. Lett., 22, 2625–2628, 1995. 10690, 10691, 10695
Ritzhaupt, G. and Devlin, J. P.: Infrared spectra of nitric and hydrochloric acid hydrate thin films, J. Phys. Chem., 95, 90–95, 1991. 10691
Rodgers, C. D.: Inverse Methods for Atmospheric Sounding: Theory and Practice, vol. 2 of Series on Atmospheric, Oceanic and Planetary Physics, edited by: Taylor, F. W., World Scientific, 2000. 10693
Scarchilli, C., Adriani, A., Cairo, F., Donfrancesco, G. D., Buontempo, C., Snels, M., Moriconi, M. L., Deshler, T., Larsen, N., Luo, B., Mauersberger, K., Ovarlez, J., Rosen, J., and Schreiner, J.: Determination of polar stratospheric cloud particle refractive indices by use of in situ optical measurements and T-matrix calculations, Appl. Opt., 44, 3302–3311, 2005. 10697, 10698
Schreiner, J., Voigt, C., Kohlmann, A., Arnold, F., Mauersberger, K., and Larsen, N.: Chemical analysis of polar stratospheric cloud particles, Science, 283, 968–970, 1999. 10687
Solomon, S.: Stratospheric Ozone Depletion: A Review of Concepts and History, Rev. Geophys., 37, 275–315, 1999. 10686
Spang, R. and Remedios, J. J.: Observations of a distinctive infra-red spectral feature in the atmospheric spectra of polar stratopsheric clouds measured by the CRISTA instrument, Geo-

phys. Res. Lett., 30, 2003. 10688, 10699, 10703
Spang, R., Remedios, J. J., Kramer, L. J., Poole, L. R., Fromm, M. D., Müller, M., Baumgarten, G., and Konopka, P.: Polar stratospheric cloud observations by MIPAS on ENVISAT: detection method, validation and analysis of the northern hemisphere winter 2002/2003, Atmos. Chem. Phys., 5, 679–692, 2005, SRef-ID: 1680-7324/acp/2005-5-679. 10688
Steck, T.: Methods for determining regularization for atmospheric retrieval problems, Appl. Opt., 41, 1788–1797, 2002. 10694
Strawa, A. W., Drdla, K., Fromm, M., Pueschel, R. F., Hoppel, K. W., Browell, E. V., Hamill, P., and Dempsey, D. P.: Discriminating Types Ia and Ib polar stratospheric clouds in POAM satellite data, J. Geophys. Res.,107(D20), SOL 34–1, 8291, doi:10.1029/2001JD000458, 2002. 10688
Tabazadeh, A., P.Turco, R., Dradla, K., Jacobson, M. Z., and Toon, O. B.: A study of type I polar stratospheric cloud formation, Geophys. Res. Lett., 21, 1619–1622, 1994. 10687
Tabazadeh, A., Jensen, E. J., Toon, O. B., Drdla, K., and Schoeberl, M. R.: Role of the stratospheric polar freezing belt in denitrification, Science, 291, 2591–2594, 2001. 10701
Tisdale, R. T., Prenni, A. J., Iraci, L. T., Tolbert, M. A., and Toon, O. B.: Variation of the infrared spectra of nitric acid hydrates with formation conditions: Impact on PSC identification, Geophys. Res. Lett., 26, 707–710, 1999. 10690, 10691, 10692
Tolbert, M. A. and Toon, O. B.: Solving the PSC Mystery, Science, 292, 61–63, 2001. 10687
Toon, O. B. and Tolbert, M. A.: Spectroscopic evidence against nitric acid trihydrate in polar stratospheric clouds, Nature, 375, 218–221, 1995. 10688
Toon, O. B., Browell, E. V., Kinne, S., and Jordan, J.: An analysis of lidar observations of polar stratospheric clouds, Geophys. Res. Lett., 17, 393–396, 1990. 10687
Toon, O. B., Tolbert, M. A., Middlebrook, A. M., and Jordan, J.: Infrared optical constants of H_2O, ice, amorphous nitric acid solutions, and nitric acid hydrates, J. Geophys. Res., 99, 25 631–25 654, 1994. 10688, 10690, 10691, 10692, 10695, 10702, 10703, 10712, 10717, 10719
Voigt, C., Schreiner, J., Kohlmann, A., Zink, P., Mauersberger, K., Larsen, N., Deshler, T., Kröger, C., Rosen, J., Adriani, A., Cairo, F., Di Donfrancesco, G., Viterbini, M., Ovarlez, J., Ovarlez, H., David, C., and Dörnbrack, A.: Nitric Acid Trihydrate (NAT) in Polar Stratospheric Clouds, Science, 290, 1756–1758, 2000. 10687
von Clarmann, T., Glatthor, N., Grabowski, U., Höpfner, M., Kellmann, S., Kiefer, M., Lin-

den, A., Mengistu Tsidu, G., Milz, M., Steck, T., Stiller, G. P., Wang, D. Y., Fischer, H., Funke, B., Gil-López, S., and López-Puertas, M.: Retrieval of temperature and tangent altitude pointing from limb emission spectra recorded from space by the Michelson Interferometer for Passive Atmospheric Sounding (MIPAS), J. Geophys. Res., 108(D23), 4736, doi:10.1029/2003JD003602, 2003. 10693

Wagner, R., Mangold, A., Möhler, O., Saathoff, H., Schnaiter, M., and Schurath, U.: A quantitative test of infrared optical constants for supercooled sulphuric and nitric acid droplet aerosols, Atmos. Chem. Phys., 3, 1147–1164, 2003, SRef-ID: 1680-7324/acp/2003-3-1147. 10692

Worsnop, D. R., Fox, L. E., Zahniser, M. S., and Wofsy, S. C.: Vapor pressure of solid hydrates of nitric acid: implications for polar stratospheric clouds, Science, 259, 71–74, 1993. 10687, 10701

Table 1. Selected matches between PSC observations by lidar from McMurdo (77.9° S/166.7° E) and by MIPAS from Envisat.

PSC Type	Lidar date/time(UT)	MIPAS date/time(UT)/lat/lon	Distance [km]
1a	4 August 2003/08:14	4 August 2003/12:02/−76.3/166.6	178
1b	15 June 2003/00:54	14 June 2003/22:01/−78.5/169.4	91
2	21 June 2003/02:20	20 June 2003/22:13/−77.5/167.6	49

ACPD
5, 10685–10721, 2005

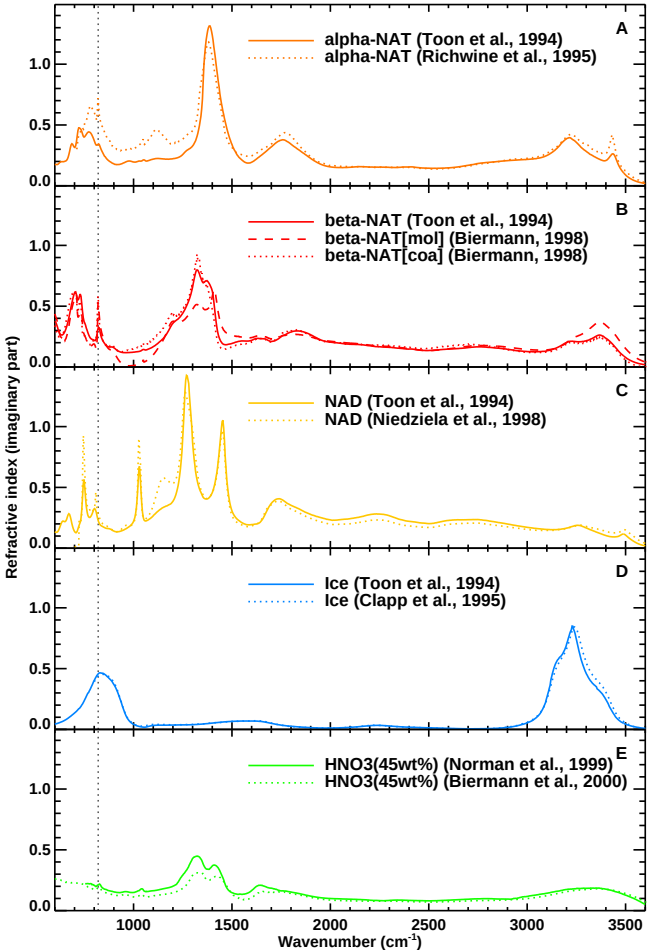

Fig. 1. Refractive indices for different PSC-candidate compositions and from various laboratory studies.

ACPD
5, 10685–10721, 2005

Evidence for β-NAT, STS, and ice from MIPAS

M. Höpfner et al.

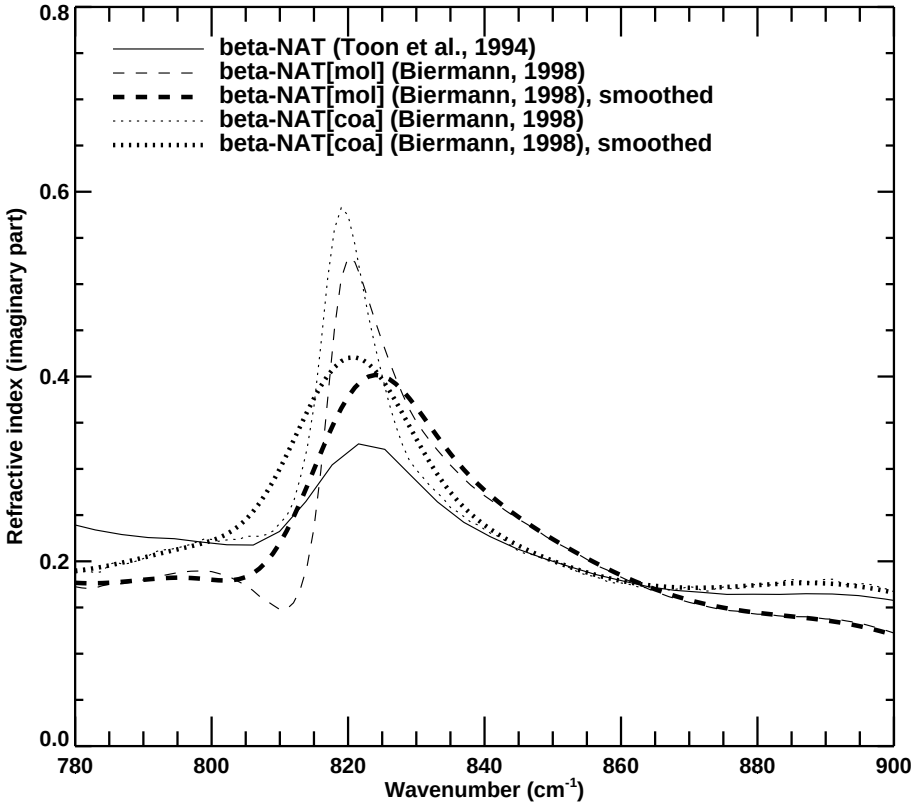

Fig. 2. The effect of reduced spectral resolution on refractive indices of β-NAT in the region of the ν_2-band of NO_3^-. Biermann (1998)'s data which have been obtained with a resolution of 1 cm^{-1} have been smoothed to be comparable with the measurements by Toon et al. (1994).

ACPD
5, 10685–10721, 2005

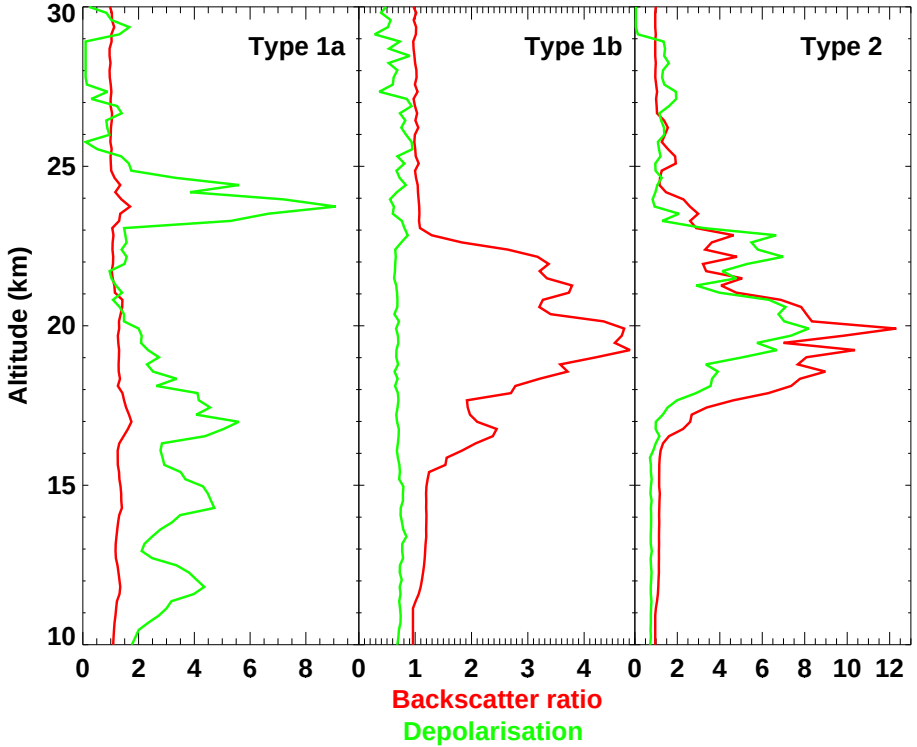

Fig. 3. Three lidar measurements of different PSC Types which were selected for analysis of PSCs in matching MIPAS limb-scans (see Table 1).

ACPD
5, 10685–10721, 2005

Evidence for β-NAT, STS, and ice from MIPAS

M. Höpfner et al.

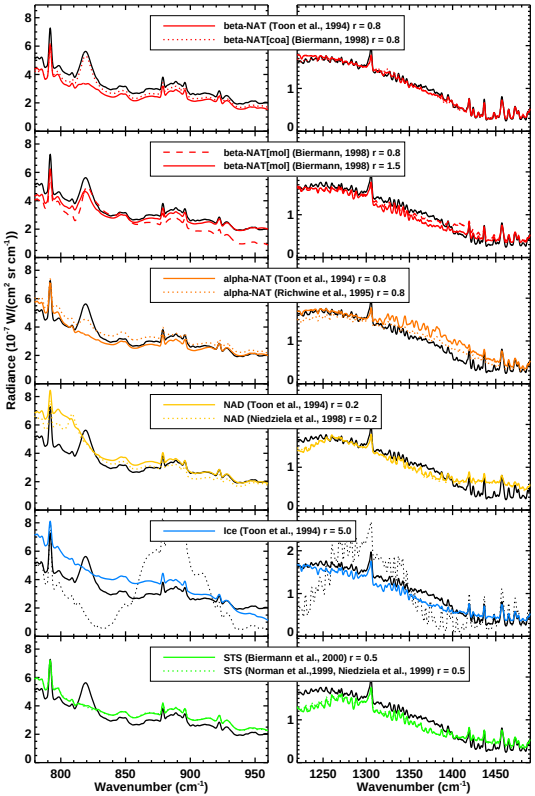

Fig. 4. MIPAS spectra for a tangent altitude of 15.2 km on 4 August 2003 (black solid, for exact geolocation see Table 1) in comparison with radiative transfer simulations for different refractive indices (color) and a nearby PSC-free measurement (black, dotted). For better visibility of the aerosol features the calculated and the MIPAS spectra have been degraded to a resolution of 1 cm^{-1}. The most prominent PSC signature in the MIPAS measurements is at 820 cm^{-1}. This PSC observation occurred close to a Lidar measurement of Type 1a clouds. Simulations shown are those resulting from the best fit of number density and mean radius (as given in the legend) based on log-normal distributions.

ACPD
5, 10685–10721, 2005

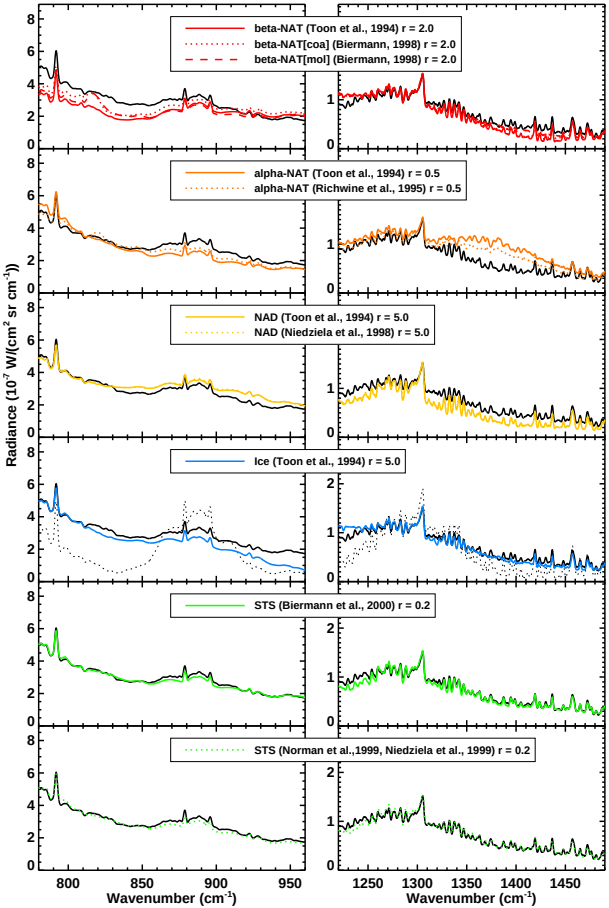

Fig. 5. Same plot as Fig. 4 but for MIPAS spectra on 14 June 2003 for a tangent altitude of 17.3 km (black) in comparison with radiative transfer simulations for different refractive indices (color) and a nearby PSC-free measurement (black, dotted). This observation occurred close to a Lidar measurement of Type 1b PSCs.

ACPD
5, 10685–10721, 2005

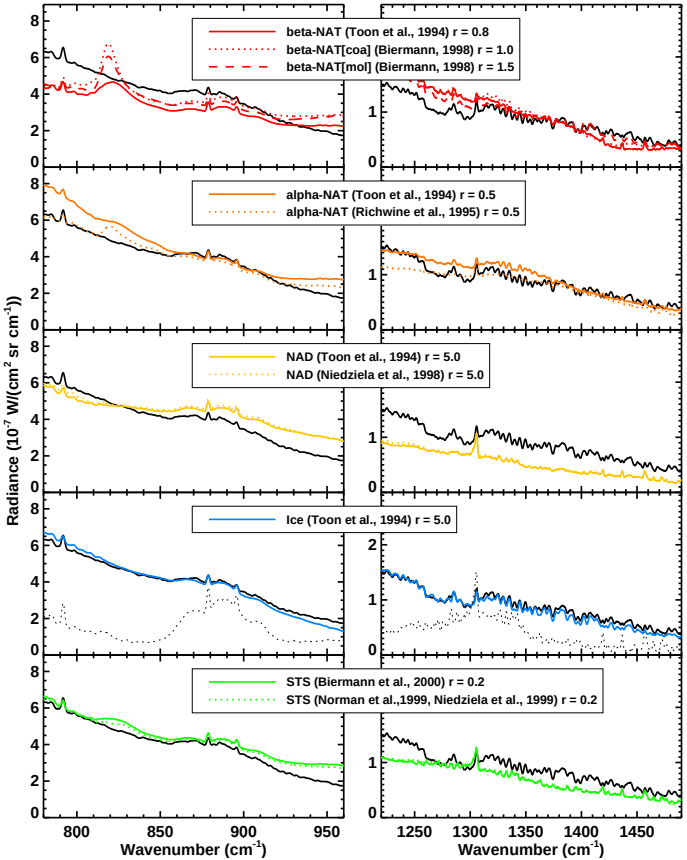

Fig. 6. Same as Fig. 4 but for MIPAS measurements on 20 June 2003 for tangent altitude 23.4 km (black). The observation occurred near a Lidar measurement of Type 2 PSCs.

ACPD
5, 10685–10721, 2005

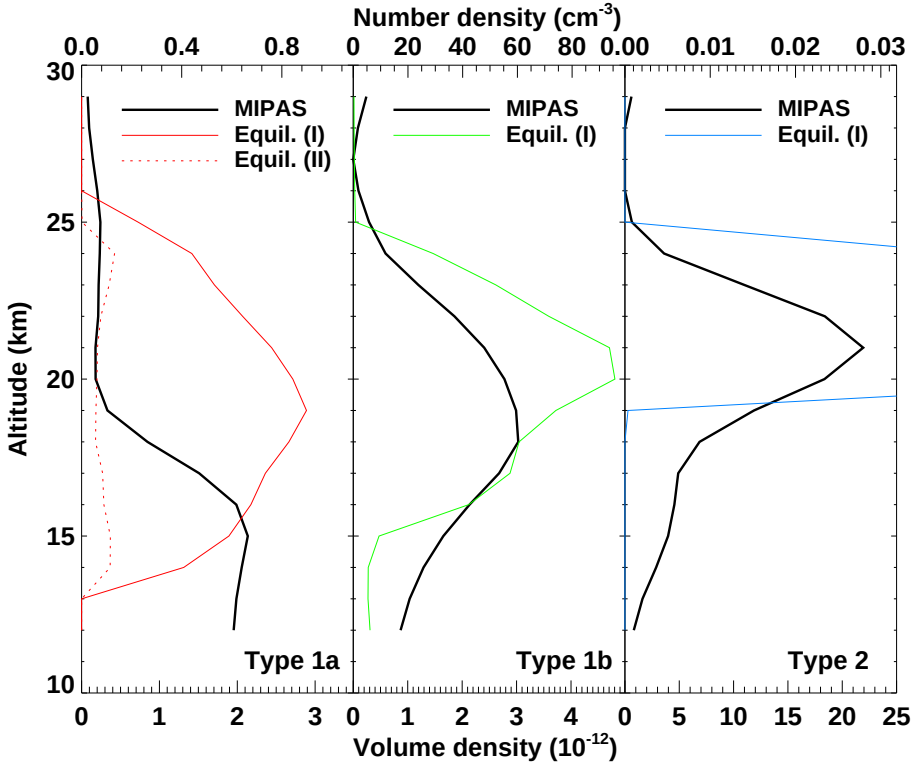

Fig. 7. MIPAS PSC retrieval of number density (black curves, top axis) for the collocations with the three different Lidar Type measurements. The results were obtained with the following settings of median radius and refractive indices. Type 1a: r_m=0.8 μm, β-NAT refractive indices by Biermann (1998) and this work; Type 1b: r=0.2 μm, refractive indices by Biermann et al. (2000); Type 2: r=5.0 μm, refractive indices by Toon et al. (1994). Volume density is calculated from N,r_m, and σ=1.35 (black curves, bottom axis). Colored curves are volume density profiles for NAT (red), STS (green), and ice (blue) in thermodynamic equilibrium (see text for details).

ACPD
5, 10685–10721, 2005

Evidence for β-NAT, STS, and ice from MIPAS

M. Höpfner et al.

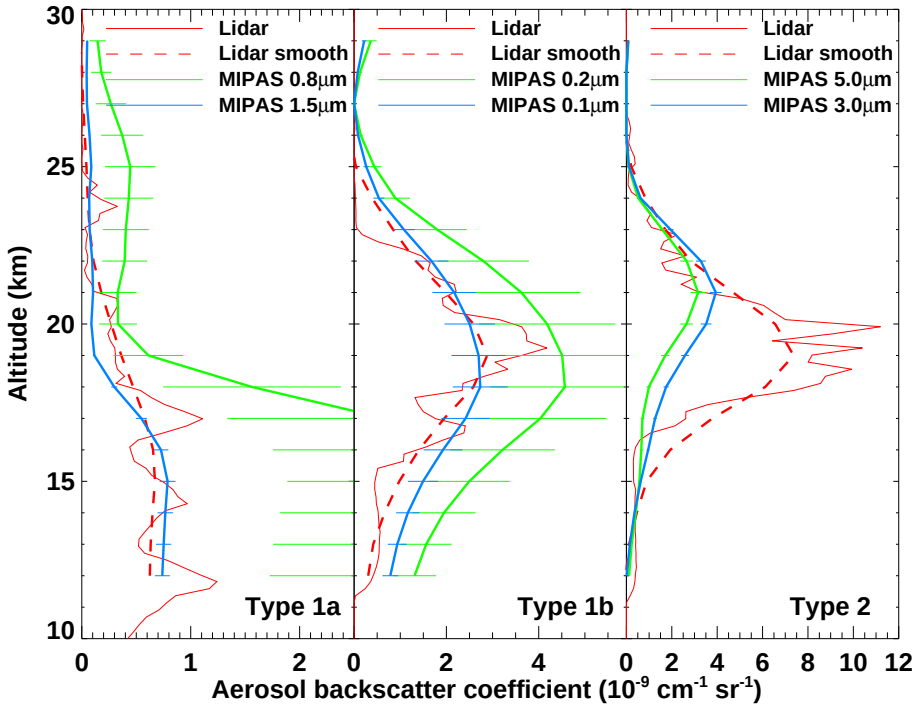

Fig. 8. Comparison of aerosol backscatter coefficients at 532 nm between Lidar measurements (red) and calculations based on MIPAS retrievals for two different median radii (green and blue). Solid red lines are the original lidar observations, while dashed ones are convolved with the averaging kernel of the MIPAS results. Error bars indicate the variation of the results for the range of refractive indices for NAT (Type 1a), STS (Type 1b), and ice (Type 2) from literature.

ACPD
5, 10685–10721, 2005

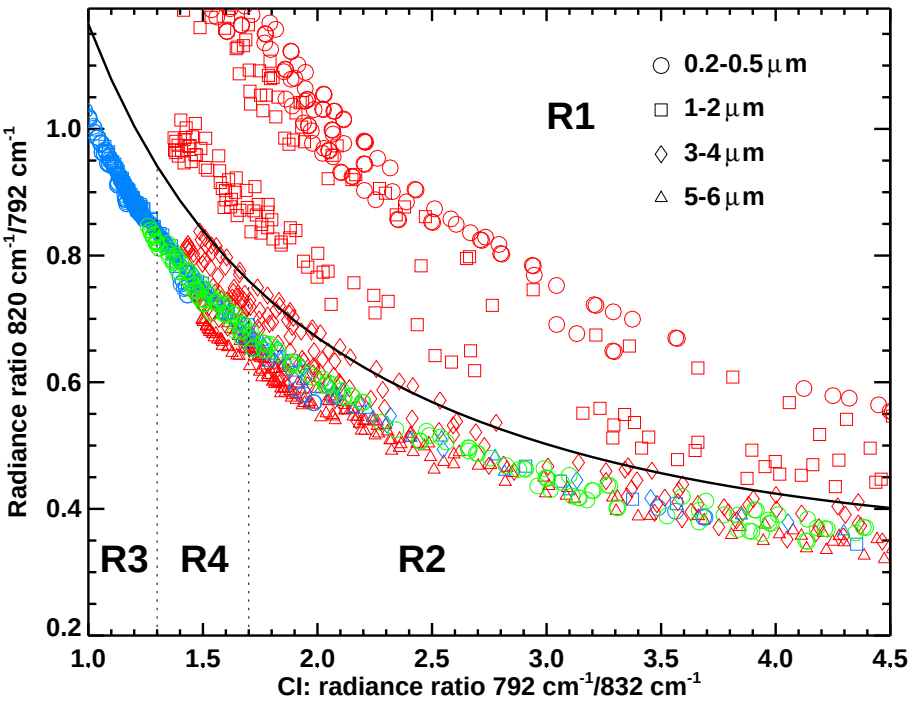

Fig. 9. Mean spectral intensity in the interval 819–821 cm^{-1} (I[819–821 cm^{-1}]) divided by I[788.2–796.25 cm^{-1}] versus I[788.2–796.25 cm^{-1}]/I[832.3–834.4 cm^{-1}] of simulated MIPAS PSC observations. For the calculations the following refractive indices have been used. β-NAT (red), (Biermann, 1998)[coa]; STS (green) (Biermann et al., 2000); ice (blue) (Toon et al., 1994). The symbols denote the mean radii used for the underlying log-normal distributions (geometric standard deviation=1.35).

ACPD
5, 10685–10721, 2005

Evidence for β-NAT, STS, and ice from MIPAS

M. Höpfner et al.

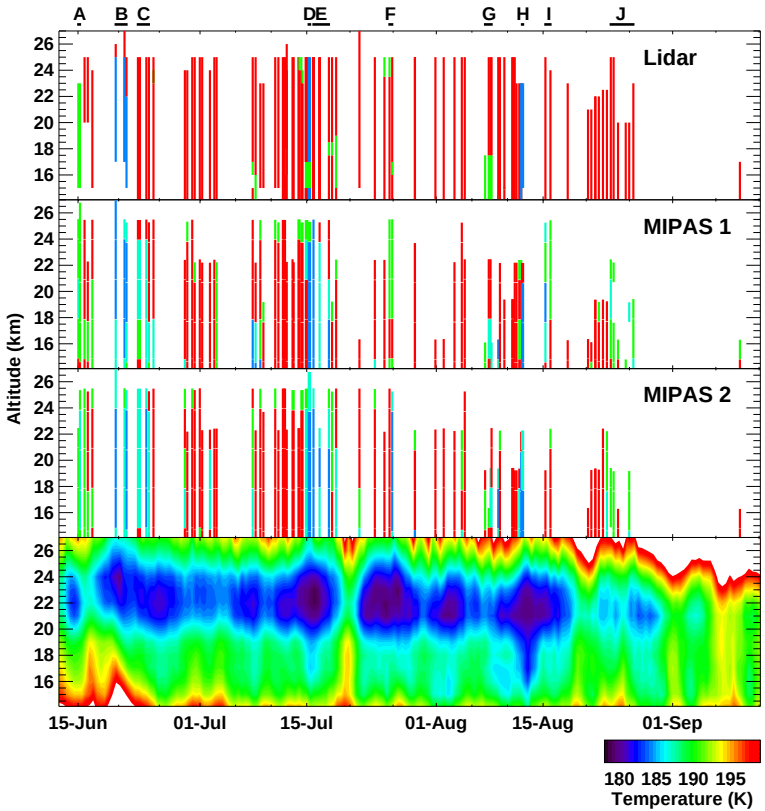

Fig. 10. Comparison between lidar and MIPAS PSC type analysis. For lidar, red indicates Type 1a, green Type 1b and blue Type 2 PSC. In case of MIPAS red stands for R1, blue for R3, green for R2, and blue-green for region R4 in Fig. 9. "MIPAS 1" indicate the nearest and "MIPAS 2" the second nearest MIPAS limb-scan with respect to the lidar observation in terms of Δtot (see text). A–J denote periods discussed in the text.

ACPD
5, 10685–10721, 2005

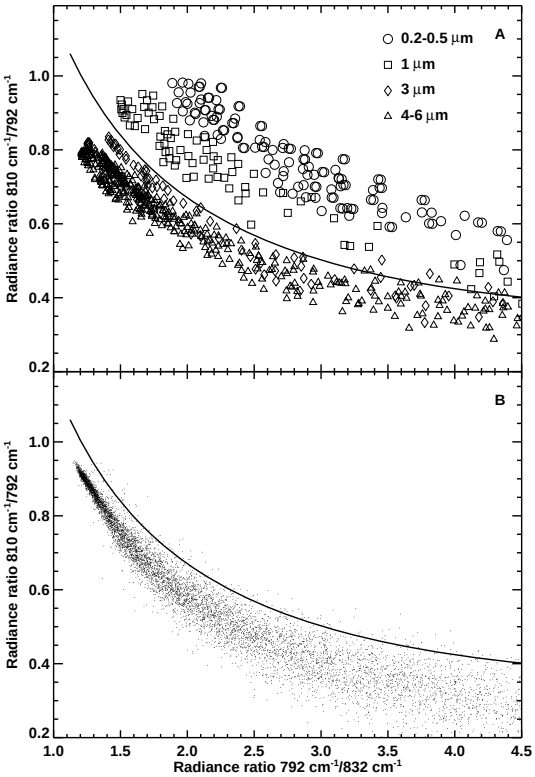

Fig. 11. Mean spectral intensity in the interval 810.05–810.35 cm^{-1} (I[810.05–810.35 cm^{-1}]) divided by I[788.2–796.25 cm^{-1}] versus I[788.2–796.25 cm^{-1}]/I[832.3–834.4 cm^{-1}] of simulated **(A)** and measured **(B)** MIPAS PSC observations to search for NAD PSCs. The calculations in A are based on refractive index data of NAD by Niedziela et al. (1998) and a variety of particle number density profiles and particle sizes. Different symbols depict different median particle radii. B: all data points from MIPAS PSC observations for tangent altitudes between 16 and 25 km from May until October 2003.

ACPD
5, 10685–10721, 2005